Research Article

Markad Kanif, Patekar Vivek*, Kale Kishor

Experimental and numerical investigation of nanomaterial-based structural composite

https://doi.org/10.1515/cls-2022-0220
received July 17, 2023; accepted November 08, 2023

Abstract: In this work, we discussed multi-phase composites fabrication and analytical as well as experimental analysis. Shear mixing of multi-walled nanotube (MWCNT) and epoxy is used to create nanocomposites. Ultrasonication, magnetic stirring, and moulding using the hand layup technique were the procedures used for sample preparation. Curing and cutting were performed as well, all in accordance with ASTM standards. This research uses an experimental method for assessing material qualities and backs up its findings with an analytical one for verification. It can be shown that the outcomes of both experiments and analyses are consistent. The structural analysis of a composite sample is probed by using a further analytical validation strategy. In this research, we examined the effects of varying the MWCNT content of the matrix. The tensile strength was shown to rise up to 0.5% MWCNT content in the matrix. For 0.7% MWCNT reinforcement in the matrix, tensile strength drops as a result of agglomeration. This research also explored the use of ANSYS for critical buckling analysis on many different multi-phase nanocomposite samples. The critical buckling resistance capability of the various configurations of composite materials was examined, and the model's efficacy was shown via validation against existing literature.

Keywords: prestine CFRP, hybrid composite, hybrid matrix, multi-phase composite, buckling analysis

*** Corresponding author: Patekar Vivek,** Mechanical Engineering Department, DVVP COEA, Maharashtra, India,
e-mail: patekar_mech@enggnagar.com
Markad Kanif: Mechanical Engineering Department, DVVP COEA, Maharashtra, India
Kale Kishor: Mechanical Engineering Department, Government Polytechnic, Pune, India

1 Introduction

The mixture's distinct qualities are a result of the interaction between its various elements. The demands of modern technology are not always met by monolithic plates and their alloys. It is only possible to meet performance requirements by merging many devices. Pioneers in the composites industry are also working to bring composites to the transportation, building, and aerospace sectors [1–6]. More recently, the public sector has come to understand the benefits of FRP composites, particularly their resistance to corrosion. It is usually preferable to utilise a mixture. For instance, in the cutthroat aviation industry, individuals are often seeking methods to lower aircraft quality without compromising the components' toughness and longevity. Composite materials may be used in place of conventional metal alloys to achieve this. Composites are more expensive, but they are more economical since they need less assembly and fuel. In order to create novel composite materials, modified fibres, and resins are combined with nanomaterials. Products using nanotechnology started to appear in the early 2000s. The polymer's hardness, fatigue and impact resistance, thermal conductivity, resistance to corrosion, and other properties are all enhanced by carbon nanotubes or other nanofillers [7–10].

Composite structures are modelled by various techniques namely hand layup, resin transfer moulding, open contact moulding, compression moulding, reaction injection moulding, injection moulding, tube rolling and filament winding, and so on [11–14]. In the development of nanocomposite carbon nanotubes and multi-wall carbon nanotubes, graphene and nanosilica play a vital role [15]. Because composite constructions are recognised to have superior mechanical qualities than steel structures, flaws in so-called hybrid structures may be altered or removed entirely. In addition, FG plates exhibit some bending, buckling, and vibrations in accordance with different shear deformation theories [16–18]. To use the fibre-reinforced polymer (FRP) composites in various applications, it is important to increase the mechanical properties by the

reinforcement of tiny particles called nanofillers in a material to create a mixture with different phases called multiphase composites [19]. In FRP, the matrix has two different purposes: i) to bind the fibres together during loading and ii) load transfer from matrix to fibre during stress concentration. The strength of the matrix is low, and to improve the strength of the reinforcement of CNT/graphene, materials that are made up of more than one type of substance or a combination of different materials are used [5,20].

Quadrini *et al.* [21] concluded that 35.7 and 15.1% enhancement was observed in flexural and tensile elastic moduli by the reinforcement of 0.3 wt% CNT as compared with the base sample. Eskizeybek *et al.* [22] noticed that the reinforcement of CNT in glass fibre epoxy decreases the tensile strength and improves flexural strength. Kaw *et al.* [20] were noticed that Young's modulus increased by 82% by the reinforcement of 5% of MWCNT into an ultrahigh molecular weight polyethylene composite film the phenomenon of agglomeration may found in composite material which will cause a reduction in mechanical properties. Agglomeration occurs due to the ineffective dispersion of enforcement of CNT/graphene in the polymer matrix [23–26]. Much literature shows that the van der Waals force of attraction between nanoparticles agglomerates it. Agglomeration reduces the material properties [19,21,27]. Ref. [16–18,28] worked on composite material reinforced with CNT to analyse the effect of the addition of CNTs on buckling behaviour and the natural frequency of conical panels subjected to combined loading. Further work was extended by Ghasemi *et al.* [29,30] to analyse the effect of agglomeration of continuously graded SWCNTs on the vibration of the laminated cylindrical shell.

Teng and co-authors [30] noticed a dynamic vulcanisation process performed on a TPI/HDPE hybrid matrix, which results in better improvement in the mechanical properties of polymer composites. Toughness, strength and electrical conductivity properties are also increased for multiphase composites by the reinforcement of CNT/graphene, etc. [31].

Tung *et al.* [32] analysed a biaxial compression and concluded that the lowest buckling load was effectively observed with a single half wave. Lal and Markad [33] analysed the different combinations of $m = 1$; $n = 1, 2, 3 \ldots$ and $n = 1$; $m = 1, 2, 3, \ldots$ and the results are obtained by applying combinations to the isotropic plates. Ko [34] analysed the buckling strength based on aspect ratio, plate boundary conditions, and hole size for the perforated MMC plates with symmetric fibre-laminated plates. Seifi *et al.* [35] studied the different boundary conditions for laminated plates to investigate the buckling strength, and they observed that non-dimensional buckling load under C–C is much high as compared with F–C and C–F boundary conditions. Pai *et al.* [36] carried out mode analysis and concluded that the debonding of the patch changes the higher mode shapes more as compared to the lower-mode shapes.

The present study focuses on CNTs' ability to improve the mechanical properties of carbon fibre–reinforced polymer CFRP hybrid composites. Proper dispersion of CNT in the matrix was made by sonication, magnetic stirring or calendaring [37,38]. The CNT concentrations are taken as 0.1, 0.3, 0.5, 0.7% Bisphenol with aliphatic Amin epoxy with reinforcement of MWCNT used for preparation of multi-phase matrix. The tensile behaviour of the hybrid composites is studied. The research looks at how strong a special kind of material is by studying analytical and experimental approaches for multiphase hybrid composites. The critical buckling load (CBL) is also investigated for samples manufactured by an analytical approach and validated by ANSYS.

2 Material properties

High-purity MWCNT with an external diameter of 10–15 nm and length of 5 μm were reinforced with bisphenol and base epoxy resin with an aliphatic amine. The carbon fibre was used in 0° ply orientation. The CNT percentage varies from 0.1, 0.3, 0.5, and 0.7%. The properties of matrix carbon fibre and CNT are enlisted in Table 1.

The evaluation of material properties was carried out by the Halpin-Tsai approach. The properties of three-phase material (i.e. matrix, carbon fibre, and MWCNT) are important for the analytical approach. The properties of three-phase laminated structures are reviewed and shortlisted from [8]. Polymer composite exhibits remarkable mechanical properties as compared to its corresponding polymer without compromising the shape memory behaviour. The enhancement of the mechanical and thermomechanical properties of the carbon fibre-reinforced polymer composite is presented in the present study with the incorporation of MWCNT in the SMP matrix. The fabrication process involved the preparation of the MWCNT/epoxy nanocomposites through ultrasonication and shear mixing and the

Table 1: Material properties of individual content

Material properties	Epoxy	MWCNT	Carbon fibre
Modulus of elasticity	3.3 GPa	1.0 TPa	230 GPa
Poisson's ratio	0.4	0.28	0.19
Number of walls in MWCNT	—	2	—

subsequent moulding of the carbon fiber-reinforced hybrid polymer composites by hand layup technique. The mechanical and thermomechanical characterisations were conducted as per the ASTM standards. The improvement of the interfacial bonding between the fibre and matrix and the wettability of carbon fibre supported these improvements. The process of fabrication includes the preparation of the MWCNT/epoxy hybrid nanocomposites by shear mixing, ultrasonication, magnetic stirring, and subsequent moulding by hand layup method. The appropriate post-processing was performed for the curing and cutting to prepare the samples for the mechanical and thermomechanical characterisations as per the ASTM standards. An enhancement in the thermomechanical properties was noticed due to the incorporation of the MWCNT. The elastic modulus of MWCNT can be evaluated from the following equations,

$$E_{\text{mwcnt}} = \frac{W_n * t_{\text{cnt}} * E_{\text{swcnt}}}{(W_n - 1) * h_{\text{in}} + t_{\text{cnt}}}. \tag{1}$$

Here, the SWCNT thickness t_{cnt} was taken as 1.5 nm and h_{in} is the MWCNT wall spacing ($h_{\text{in}} = 1.5 \times t_{\text{cnt}}$). W_n indicates the number of walls of CNT.

$$E_{\text{ecnt}} = \frac{2 \times t_{\text{cnt}} \times E_{\text{mwcnt}}}{r_{\text{cnt}}}, \tag{2}$$

where E_{mwcnt}, t_{cnt} and r_{cnt} are Young's modulus of MWCNT, nanotube wall thickness, and radius of nanotube, respectively.

$$E_{\text{mcnt}} = \left(\frac{3 \times E_{\text{m}}}{8}\right) \times \frac{[(1 + \text{GTL} \times V_{\text{cnt}} \times A)]}{[(1 - V_{\text{cnt}} \times A)]} + \left(\frac{5 \times E_{\text{m}}}{8}\right) \frac{[(1 + GTT \times V_{\text{cnt}} \times B)]}{[(1 - V_{\text{cnt}} \times B)]}, \tag{3}$$

where $A = \frac{\left\{\left(\frac{E_{\text{ecnt}}}{E_{\text{m}}}\right) - 1\right\}}{\left\{\frac{E_{\text{ecnt}}}{E_{\text{m}}} + \text{GTL}\right\}}$, $B = \frac{\left\{\left(\frac{E_{\text{ecnt}}}{E_{\text{m}}}\right) - 1\right\}}{\left\{\frac{E_{\text{ecnt}}}{E_{\text{m}}} + \text{GTT}\right\}}$.

$$G_{\text{mcnt}} = \left(\frac{E_{\text{m}}}{8}\right) \times \frac{[(1 + \text{GTL} \times V_{\text{cnt}} \times C)]}{[(1 - V_{\text{cnt}} \times C)]} + \left(\frac{E_{\text{m}}}{4}\right) \times \frac{[(1 + \text{GTT} \times V_{\text{cnt}} \times D)]}{[(1 - V_{\text{cnt}} \times D)]}, \tag{4}$$

where $C = \frac{\left\{\left(\frac{E_{\text{ecnt}}}{E_{\text{m}}}\right) - 1\right\}}{\left\{\frac{E_{\text{ecnt}}}{E_{\text{m}}} + \text{GTL}\right\}}$, $D = \frac{\left\{\left(\frac{E_{\text{ecnt}}}{E_{\text{m}}}\right) - 1\right\}}{\left\{\frac{E_{\text{ecnt}}}{E_{\text{m}}} + \text{GTT}\right\}}$.

$$\mu_{\text{mcnt}} = \frac{E_{\text{mcnt}}}{2 \times G_{\text{mcnt}}} - 1, \tag{5}$$

GTL = $(2 \times l)/d$, where l = 5,000 nm and d = 15 nm being the length and diameter of the nanotube.

$E_1 = (E_{\text{f}} \times V_{\text{f}}) + (E_{\text{mcnt}} \times V_{\text{m}})$

$$\mu_{12} = (\mu_{\text{f}} \times V_{\text{f}}) + (\mu_{\text{mcnt}} \times V_{\text{m}}), \tag{6}$$

$$E = \frac{\left\{\left(\frac{E_{\text{f}}}{E_{\text{m}}}\right) - 1\right\}}{\left\{\frac{E_{\text{f}}}{E_{\text{m}}} + 2\right\}}, \; F = \frac{\left\{\left(\frac{G_{\text{f}}}{G_{\text{m}}}\right) - 1\right\}}{\left\{\frac{G_{\text{f}}}{G_{\text{m}}} + 1\right\}},$$

$$E_2 = E_m = \frac{[(1 + 2 \times V_{\text{f}} \times E)]}{[(1 - V_{\text{f}} \times E)]}, \tag{7}$$

$$G_{12} = G_{23} = G_{\text{m}} = \frac{[(1 + V_{\text{f}} \times F)]}{[(1 - V_{\text{f}} \times F)]}, \tag{8}$$

$$H = \frac{\left\{\left(\frac{\mu_{\text{f}}}{\mu_{\text{m}}}\right) - 1\right\}}{\left\{\frac{\mu_{\text{f}}}{\mu_{\text{m}}} + 1\right\}},$$

$$\mu_{23} = \mu_{\text{m}} = \frac{[(1 + V_{\text{f}} \times H)]}{[(1 - V_{\text{f}} \times H)]}, \tag{9}$$

where V_{f} and V_{m} are carbon fibre and matrix volume fractions, respectively. Young's modulus of the unidirectional lamina in longitudinal and transverse directions is represented by E_1, E_2. Poisson's ratio μ_{12} was evaluated by the rule of mixture. G_{12}, G_{23} are the shear modulus evaluated by using the mixture rule.

3 Sample preparation

In this work, two types of samples were prepared as follows:

1. Pure CFRP,
2. CFRP with reinforcement of MWCNT.

3.1 Preparation of CFRP

For the preparation of CFRP, the hand layup technique was used. Initially, carbon fibres were laid on the mould, and then, the epoxy resin was applied on fibres as per the guidelines of the manufacturer epoxy resin and hardener mixing ratio is maintained at 100:10. In hand layup technique excessive resins can be extracted by roller moving in the direction of fibre orientation. By pressing the roller over the fibre along with excessive resins voids also get removed. Uniform pressure is applied on the sample and kept for 24 h at room temperature. In the next part of curing, the sample is heated up to 80°C in the oven which will help to remove air trapped in the sample during preparation [5,6]. The volume fraction of carbon fibre is maintained at 28%, which will ensure the interferential bond between fibre and epoxy matrix.

3.2 Preparation of CFRP with MWCNT reinforcement

Initial MWCNT were dispersed in 100 ml acetone and stirred for 1 h and then followed by sonication for 10 min. The purpose of this mixing is to do a de-agglomeration of MWCNT nanoparticles. In the sonication process, the temperature may rise to an undesirable level that may cause the rupture of walls of nanoparticles; therefore, it is necessary to keep the specimen surrounded by ice bath. The sonicated mixture, i.e. acetone and MWCNT, was added to epoxy resin and stirred at 2,000 rpm at 85°C; during this stage, the acetone was turned into a gas and went away from the mixture. The remaining mixture is again sonicated for 1 h which will cause uniform distribution of MWCNT in resin. After the sonication process, the mixture is kept in a vacuum chamber for 24 h to release air bubbles from the mixture which will be created by the sonicator. The hardener was added to the mixture of resin and MWCNT which was stirred for 10 min; five layered specimen were prepared by varying weight percentages of MWCNT as 0, 0.1, 0.3, 0.5 and 0.7%. Later, samples were machined by an abrasive water jet machine for the required tensile test. A schematic representation of the fabrication of CFRP with MWCNT is shown in Figure 1.

3.3 Material characterisation

The burnoff test was performed in accordance with ASTMD 3171-99 and was used to ascertain the samples' levels of fibre content. In the course of this procedure, 25 mm × 25 mm samples were subjected to a weight measurement to determine the starting weight. The object is then put into an oven at a temperature of 625°C for 5 h, during which time both the epoxy glue and the air trap will degrade from the sample.

Tensile tests were carried out on nanoparticle composite samples as per ASTM D3039. Sample dimensions are 150 mm × 20 mm × 1.8 mm which was performed on Instron UTM 5582. The Instron UTM5582 from ARAI in Pune, India, was used to carry out these tests. It has a load capacity of 100 kN and a measuring speed of 5 mm/min.

4 Results and discussion: Experimental

4.1 Fibre volume fraction

Fibre volume fractions are shown in Figure 2. The void content of the sample causes a noticeable shift in the

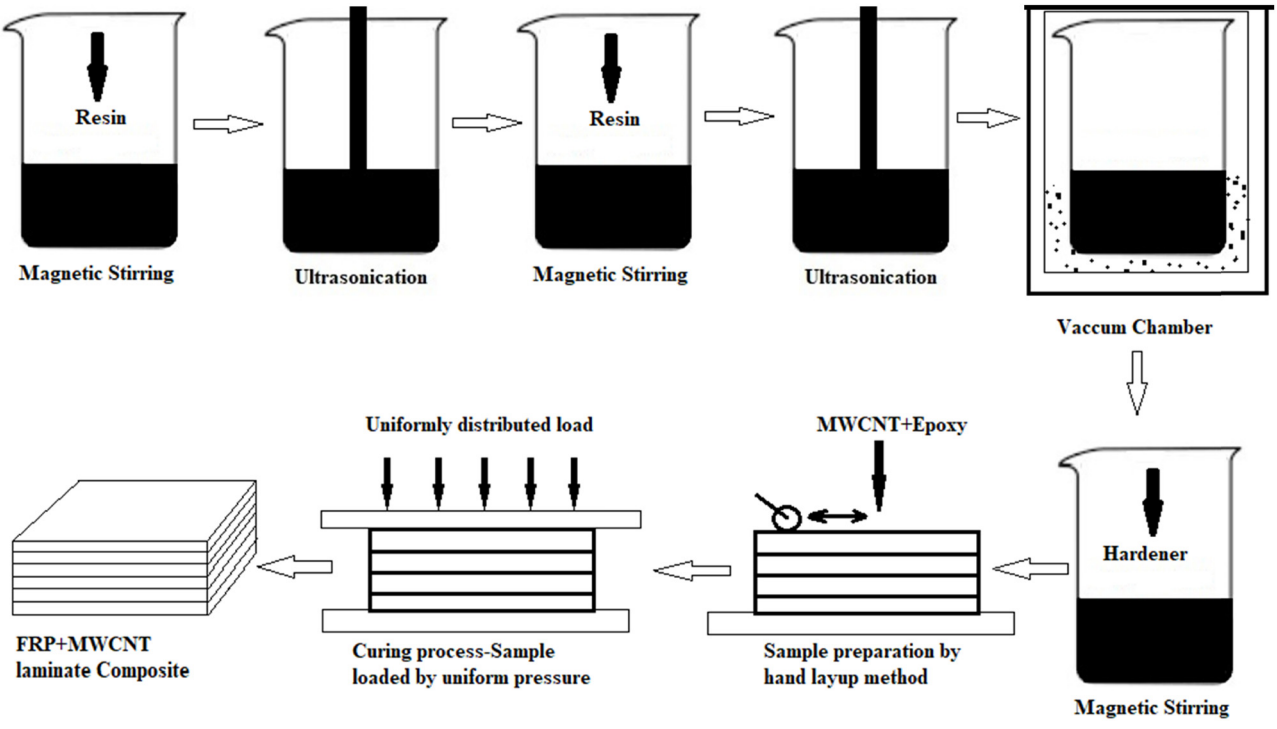

Figure 1: Schematic diagram to represent fabrication of CFRP with MWCNT.

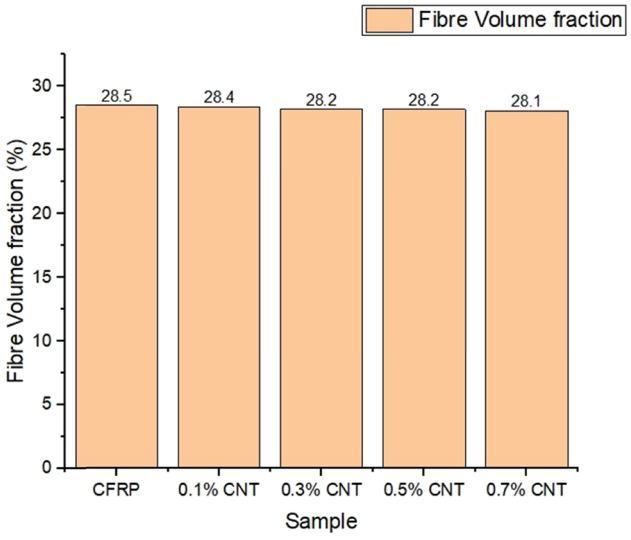

Figure 2: Fiber volume fraction in CFRP with MWCNT.

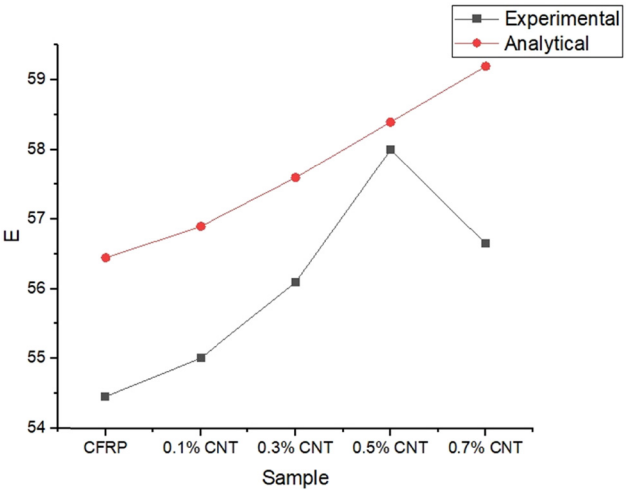

Figure 4: Modulus of elasticity for reinforced sample containing varying % of MWCNT.

volume fraction. These crevices appeared in a vacuum chamber while storing a sonicated sample of epoxy resin enhanced with MWCNT. Not all Bubbles are destroyed before they reach the matrix [6,39]. The carbon fibre's volume proportion stayed about the same, at around 28%.

4.2 Tensile test

Figures 3–6 depict the tensile characteristics of the carbon fibre–reinforced MWCNT-modified nanocomposites for varying MWCNT contents. The force–displacement plots for samples with different amounts of MWCNT at room temperature are shown in Figure 3. As can be seen from the results, the produced polymer MWCNT samples have a higher load-carrying capability than the pure CFRP samples. The force–displacement plot varies according to the proportion of MWCNT used to strengthen the sample, as seen in the figure. As can be shown in Figure 3, the MWCNT-reinforced polymer has a higher load-bearing capability than the CFRP sample. Modified nanocomposites containing 0.1, 0.3, 0.5, and 0.7% MWCNT increased tensile strength by 9, 17, 35, and 26%, respectively, as compared to pure CFRP. Tensile parameters including maximum force, elasticity, and poisons ratio all improved with increasing CNT percentage as shown in Figures 4 and 5.

The 0.7% MWCNT sample showed a decrease in tensile strength compared to the 0.5% MWCNT sample. This runs

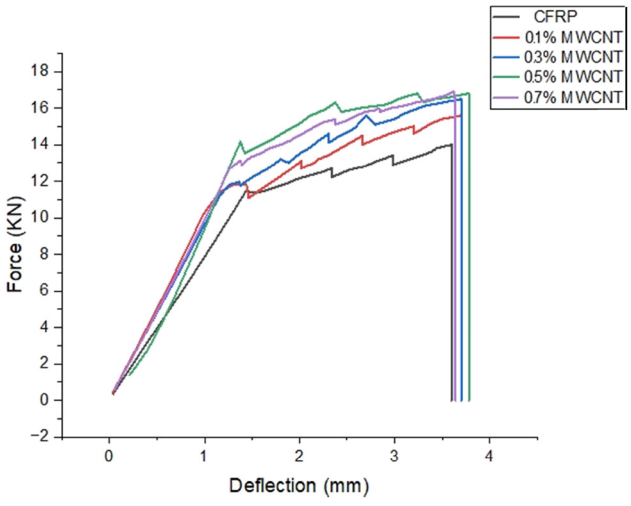

Figure 3: Tensile behaviour of reinforced sample containing varying % of MWCNT showing force vs deflection.

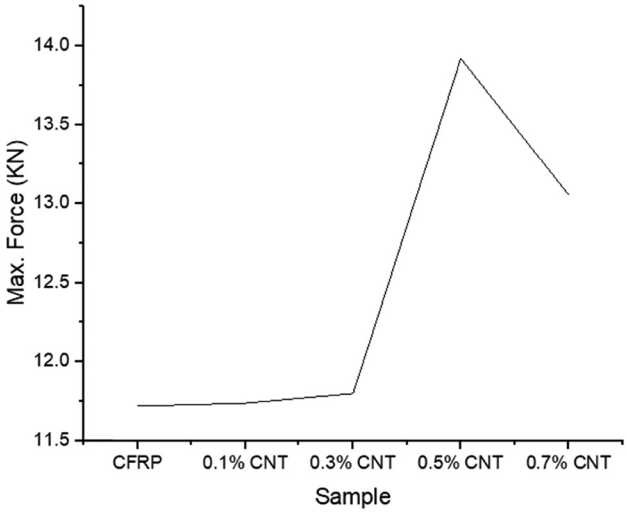

Figure 5: Force carrying capacity of reinforced sample containing different % of MWCNT.

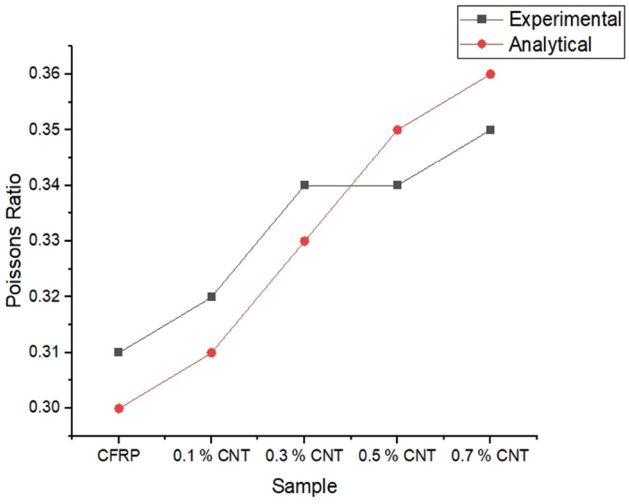

Figure 6: Poisson's ratio of reinforced sample containing different % of MWCNT.

Figure 7: Schematic representation of simply supported edges with buckling load.

counter to the trend of rising interfacial tension between CNTs and their supporting matrix. The MWCNT aggregation in the matrix was a major factor in this [40]. Because of the potential for agglomeration, MWCNT should not be introduced in excess of a certain concentration. Figure 6 contrasts the elastic characteristics determined experimentally with those determined analytically. The existence of voids or agglomerated nanoparticle bundles in the matrix accounts for the small amount of variance seen in the findings; 0.7% of the MWCNT reinforced sample showed a significant drop in mechanical characteristics, which was traced to the onset of agglomeration.

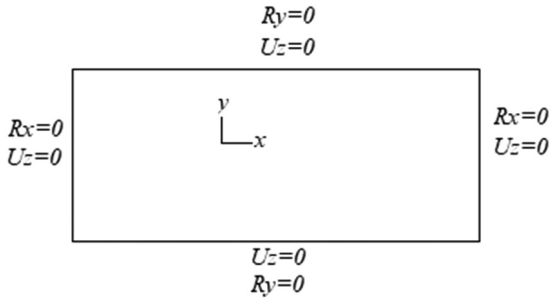

Figure 8: Boundry condition for FEA model.

5 Buckling analysis of structural composites: Analytical approach

The amount of carbon nanotubes (CNTs), plate thickness, fibre orientation, and boundary condition all have a role in the force required to cause a laminated plate to buckle [41]. Most loads are carried by continuous fibres aligned parallel to the direction of a force acting. In this study, we use both an analytical technique and a finite element method to determine the critical buckling stress for a fibre-reinforced material with a changing fraction of carbon nanotubes. For the buckling analysis, a simply supported boundary condition is used with the fibre orientation of the laminated plates held constant at 0 degrees and a compressive line pressure of 1 N/mm supplied. The characteristics of the S–S–S–S boundary condition are shown in Figure 7. The rectangular plate of length a, width b, and thickness h is acted by simply supported conditions on each edge as shown in Figure 7. A uniformly distributed load is applied on its edges as shown in the figure. The boundary conditions applied are as follows:

The governing equation for the nonlinear static analysis is

$$[K]\{q\} = \lambda[K_g]\{q\}, \qquad [10]$$

where $\{q\}$ is the transverse deflection.

$[K] = \{[K_L] + [K_{NL}] + [K_{fL}] + [K_{fNL}]\}$.

Table 2: Comparison of critical buckling load evaluated by analytical and FEM approach

Sample	Critical buckling load (N)	
	Finite element approach	Analytical approach
Pure CFRP	614.24	609.72
CFRP with reinforcement of 0.1% MWCNT	620.43	619.29
CFRP with reinforcement of 0.3% MWCNT	643.45	641.38
CFRP with reinforcement of 0.5% MWCNT	660.37	658.27

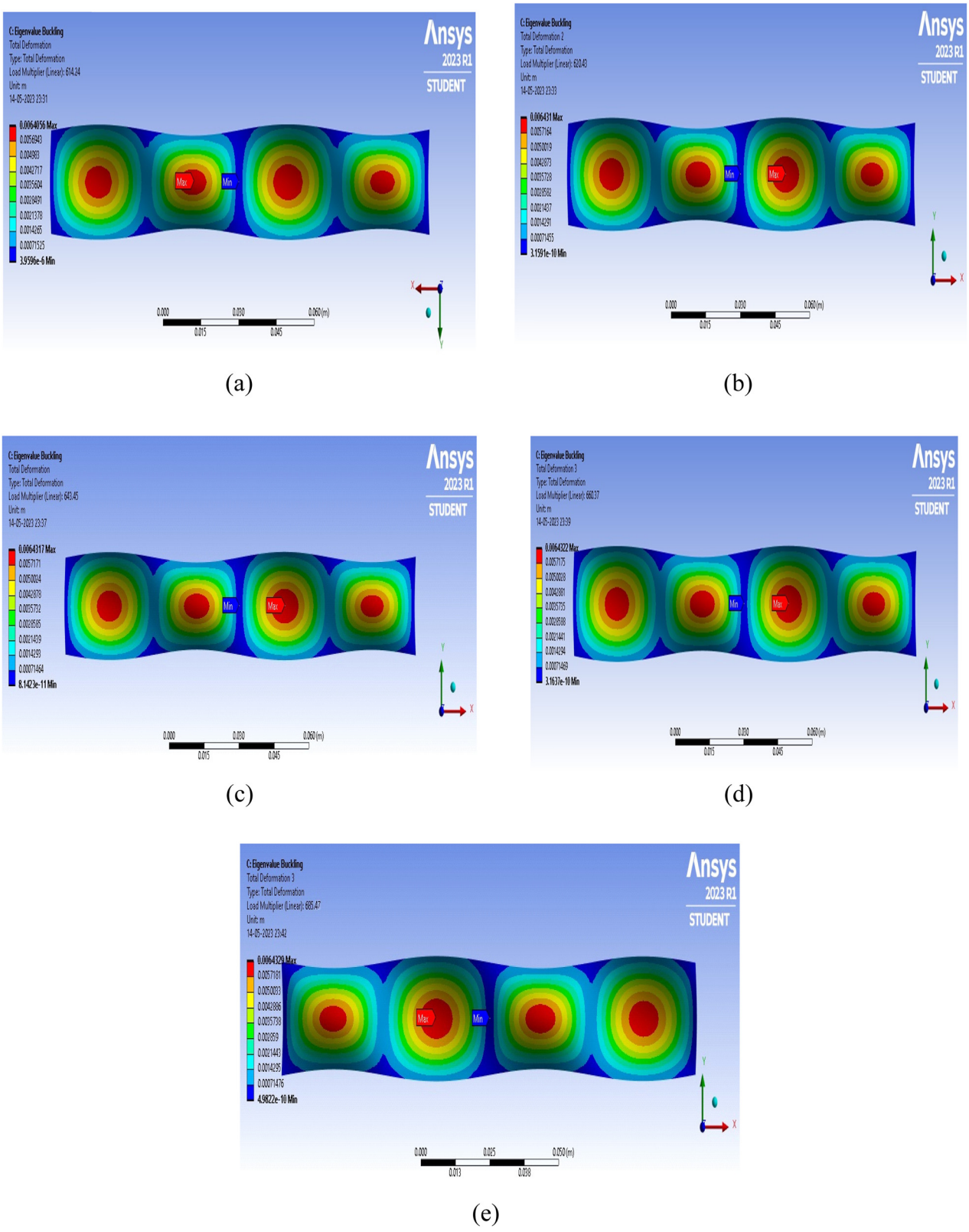

Figure 9: Buckling mode shape evaluation for (a) the presine CFRP, (b) 0.1%, (c) 0.3%, (d) 0.5% and (e) 0.7% MWCNT content in modified matrix multi-phase.

Table 3: Effect of CNT volume fraction and loading on critical buckling load

Type of loading	Ply orientation	Critical buckling load			
		0.0%	0.1%	0.3%	0.5%
Symmetric					
UDL	[0/90/0/90/0]	458.85	462.87	470.49	477.67
	[0/45/0/45/0]	504.46	509.29	518.05	526.15
	[0/30/0/30/0]	622.63	628.78	639.78	649.78
	[0/15/0/15/0]	553.97	559.48	569.29	578.26
UVL	[0/90/0/90/0]	4868.5	4919.1	5008.2	5090.3
	[0/45/0/45/0]	4779.4	4833.7	4932.1	5019
	[0/30/0/30/0]	4981.4	5043	5155	5250.9
	[0/15/0/15/0]	4852.1	4937.1	5097	5225.9
POINT LOAD	[0/90/0/90/0]	9121.9	9201.7	9353.3	9495.9
	[0/45/0/45/0]	9919.6	10016	10191	10352
	[0/30/0/30/0]	10693	10843	11064	11247
	[0/15/0/15/0]	9371.6	9539.5	9855.3	10109
Asymmetric					
UDL	[0/90/0/-90/0]	458.85	462.87	470.49	477.67
	[0/45/0/-45/0]	626.85	638.27	658.74	672.17
	[0/30/0/-30/0]	591.65	597.06	606.74	615.64
	[0/15/0/-15/0]	529.65	534.56	543.25	551.34
UVL	[0/90/0/-90/0]	9121.9	9201.7	9353.3	9495.9
	[0/45/0/-45/0]	10202	10319	10521	10697
	[0/30/0/-30/0]	9749.3	9916.5	10227	10478
	[0/15/0/-15/0]	9031.2	9198.8	9512.9	9764
POINT LOAD	[0/90/0/-90/0]	4868.5	4919.1	5008.2	5090.3
	[0/45/0/-45/0]	5087.7	5164.9	5301.9	5413.7
	[0/30/0/-30/0]	4835.4	4922.2	5087.4	5219.1
	[0/15/0/-15/0]	4685.3	4770.9	4933	5062.9

The stiffness matrix [K] is a group of different stiffness matrices that are used to measure how stiff a beam or foundation is, and there is also a geometric stiffness matrix [K_g] included. The solution to Eq. (12) can be using methods like direct iterative, incremental, or Newton–Raphson. The Newton–Raphson method is a fast and popular way to solve problems, especially when the answers are at higher amplitude.

The CBL acting on the plate is calculated by following the equation [42]:

$$\begin{aligned} \text{Ncr} = &-(\pi a/m)^2 \times (D_1 \times (m/a)^4 \\ &+ 2 \times D_3 \times (m/a)^2(n/b)^2 + D_2 \times (n/b)^4), \end{aligned} \quad [11]$$

where m is the h alf wave number along transverse direction, and n is the h alf wave number along the longitudinal direction.

where 'D' values are calculated as follows:

$D_1 = D_{11}$; $D_2 = D_{22}$; $D_3 = D_{12} + 2 \times D_{66}$

$$D_{ij} = \begin{bmatrix} D11 & D12 & D16 \\ D12 & D22 & D26 \\ D16 & D26 & D66 \end{bmatrix},$$

$$D_{\text{ij}} = \left(\frac{1}{3}\right) \times \sum_{k=1}^{n} (Q_{ij})\text{k} \times [(h^3)\text{k} - (h^3)\text{k} - 1],$$

$$Q_{11} = Q_{11} \times m^4 + 2 \times (Q_{12} + 2 \times Q_{66})m^2n^2 + Q_{22} \times n^4,$$
$$Q_{12} = Q_{12} \times (m^4 + n^4) + (Q_{11} + Q_{22} - 4 \times Q_{66})m^2n^2,$$
$$Q_{22} = Q_{11} \times n^4 + 2 \times (Q_{12} + 2 \times Q_{66})m^2n^2 + Q_{22} \times m^4,$$
$$Q_{11} = (\text{E}_{11}/(1 - \mu_{12} \times \mu_{21})),$$
$$Q_{22} = (\text{E}_{22}/(1 - \mu_{12} \times \mu_{21})),$$
$$Q_{12} = Q_{21} = (\text{E}_{11} \times \mu_{21}/(1 - \mu_{12} \times \mu_{21})),$$
$$Q_{66} = \text{G}_{12}.$$

5.1 Finite element model for buckling analysis

A total of 1,183 nodes and 1,080 elements were used in finite element analyses. CBLs (Nx,cr) were obtained from the composite plate for the first mode shape (i = 1) of each sample which is CFRP and CFRP reinforced with varying percentages of CNT. The boundary conditions applied are shown in Figure 8.

5.2 Results and discussion: buckling analysis

The CBL for the first mode shape of various samples prepared was evaluated by analytical as well as FEM. The results are listed in Table 2. It is noticed that the results are in good agreement with each other, and the error is less than 5%.

The present analysis is also focused on the buckling mode shape evaluation for each sample means for the

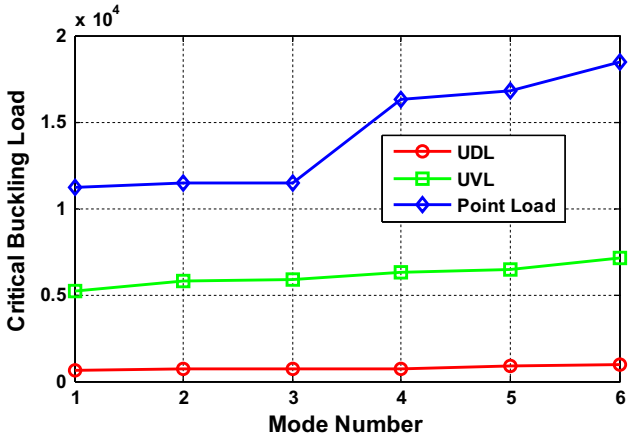

Figure 10: Variation in critical buckling load for various loading conditions.

prestine CFRP, 0.1, 0.3, 0.5, and 0.7% MWCNT content in modified matrix multi-phase samples as shown in Figure 9.

Table 3 shows the CBL investigation for the beam having an aspect ratio of 10 and a thickness ratio of 80 under simply supported boundary conditions. Various loads are applied during an investigation like uniformly distributed load (UDL), uniformly varying load (UVL), and point load over the composite beam of symmetric laminate and asymmetric laminates of five layers. Matrix of the composite material gets improved with the addition of MWCNT with CNT volume fractions of 0.1, 0.3, and 0.5% of matrix content. From the observation, it is clear that the critical buckling resistance offered by point load is maximum than any other load. The percentage of critical buckling resistance offered by point load is 93% higher than UDL, whereas it is 54% higher than UVL. In other words, we can say that UDL is the critical load where we get the lowest resistance against buckling as compared to UVL and point load.

In the previous table, the effect of various loading was examined over CNT-reinforced multi-phase composites and observed that maximum resistance to buckling was offered by multi-phase composite with 0.5% CNT content with ply orientation of [0/30/0/30/0] in the symmetric case and [0/45/0/45-/0] in asymmetric case. Further variation in critical buckling modes for various loading conditions for the beam configuration is shown in Figure 10. It also clarifies that the under UDL type of loading condition beam exhibits the lowest CBL while maximum CBL is observed in CNT-reinforced multi-phase composite beam under point load. Various buckling modes are presented in Figure 10.

6 Conclusions

Critical buckling analysis and the effect of CNT volume fraction variation on material properties and loading characteristics of CNT-reinforced multi-phase composite beams have been investigated in the present study. There is a strong correlation observed between experimental and analytical findings. The difference between these findings was less than 5% which shows the correctness of the prepared analytical model. Modified nanocomposites containing 0.1, 0.3, 0.5, and 0.7% MWCNT increased tensile strength by 9, 17, 35, and 26%, respectively, as compared to pure CFRP. But it is also found that the elastic characteristics and load-bearing capacity decrease for the 0.7% MWCNT-reinforced multi-phase composite sample. This occurs mainly due to the CNT in the mixture clumping together and forming agglomeration. This article also explored critical buckling analysis of many distinct types of multi-phase nanocomposites. The critical buckling load is found to rise with the % of CNT reinforcement, as predicted by both the analytical result and the FEA result. The effect of various loading was examined over CNT-reinforced multi-phase composites and observed that maximum resistance to buckling was offered by multi-phase composite with 0.5% CNT content with ply orientation of [0/30/0/30/0] in symmetric case and [0/45/0/45/0] in asymmetric case. The presented results also clarify that the under UDL type of loading condition beam exhibits the lowest CBL while maximum CBL is observed under point load.

Funding information: The authors received no financial support for the research, authorship, and/or publication of this article.

Conflict of interest: The authors declared no potential conflicts of interest with respect to the research, authorship, and/or publication of this article.

Author contributions: All authors have accepted responsibility for the entire content of this manuscript and approved its submission.

Data availability statement: All data that support the findings of this study are included within the article (and any supplementary files).

References

[1] Seibert HF. Applications for PMI foams in aerospace sandwich structures. Reinf Plast. 2006 Jan 1;50(1):44–8.
[2] Kim KJ, Rhee MH, Choi BI, Kim CW, Sung CW, Han CP, et al. Development of application technique of aluminum sandwich sheets for automotive hood. Int J Precis Eng Manuf. 2009 Oct 1;10(4):71–5.
[3] Tözüm TF, Keçeli HG. Treatment of peri-implant defect with modified sandwich bone augmentation. Case report and follow-up. N Y State Dent J. 2008;74(4):52–7.
[4] Karabulut G, Beköz Üllen N. A review on welding techniques of metallic foams. Erzincan Üniversitesi Fen Bilim Enstitüsü Derg. 2022 Mar 27;15(1):217–32.
[5] Tiwari N, Shaikh AA. Hybridization of carbon fiber composites with graphene nanoplatelets to enhance interfacial bonding and thermomechanical properties for shape memory applications. Polym-Plast Technol Mater. 2022 Jan 22;61(2):161–75.
[6] Markad K, Lal A. Experimental investigation of shape memory polymer hybrid nanocomposites modified by carbon fiber

reinforced multi-walled carbon nanotube (MWCNT). Mater Res Express. 2021 Oct 1;8:105015.
[7] Abaci S, Nessark B. Characterization and corrosion protection properties of composite material (PANI + TiO2) coatings on A304 stainless steel. J Coat Technol Res. 2015 Jan;12(1):107–20.
[8] Lal A, Markad K. Nonlinear flexural analysis of sandwich beam with multi walled carbon nanotube reinforced composite sheet under thermo-mechanical loading. Curved Layer Struct. 2020 Jan 1;7(1):1–16.
[9] Gimenes Benega MA, Silva WM, Schnitzler MC, Espanhol Andrade RJ, Ribeiro H. Improvements in thermal and mechanical properties of composites based on epoxy-carbon nanomaterials - A brief landscape. Polym Test. 2021 Jun 1;98:107180.
[10] Daikh AA, Houari MSA, Karami B, Eltaher MA, Dimitri R, Tornabene F. Buckling analysis of CNTRC curved sandwich nanobeams in thermal environment. Appl Sci. 2021 Jan;11(7):3250.
[11] Cetiner S, Kalaoglu F, Karakas H, Sezai Sarac A. Characterization of conductive poly(acrylonitrile-co-vinyl acetate) composites: Matrix polymerization of pyrrole derivatives. Fibers Polym. 2011 Apr 1;12(2):151–8.
[12] Nasouri K. Fabrication of lightweight and flexible cellulose acetate composite nanofibers for high-performance ultra violet protective materials. Polym Compos. 2019;40(8):3325–32.
[13] Saiah R, Sreekumar PA, Gopalakrishnan P, Leblanc N, Gattin R, Saiter JM. Fabrication and characterization of 100% green composite: Thermoplastic based on wheat flour reinforced by flax fibers. Polym Compos. 2009 Nov;30(11):1595–600.
[14] Yang D, Tu S, Chen J, Zhang H, Chen W, Hu D, et al. Phase change composite microcapsules with low-dimensional thermally conductive nanofillers: Preparation, performance, and applications. Polymers. 2023 Jan;15(6):1562.
[15] Patekar V, Kale K. State of the art review on mechanical properties of sandwich composite structures. Polym Compos. 2022;43(9):5820–30.
[16] Kiani Y, Dimitri R, Tornabene F. Free vibration study of composite conical panels reinforced with FG-CNTs. Eng Struct. 2018 Oct 1;172:472–82.
[17] Sofiyev AH, Tornabene F, Dimitri R, Kuruoglu N. Buckling behavior of FG-CNT reinforced composite conical shells subjected to a combined loading. Nanomaterials. 2020 Mar;10(3):419.
[18] Tornabene F, Fantuzzi N, Bacciocchi M, Viola E. Effect of agglomeration on the natural frequencies of functionally graded carbon nanotube-reinforced laminated composite doubly-curved shells. Compos Part B Eng. 2016 Mar 15;89:187–218.
[19] Li Q, Zaiser M, Blackford JR, Jeffree C, He Y, Koutsos V. Mechanical properties and microstructure of single-wall carbon nanotube/elastomeric epoxy composites with block copolymers. Mater Lett. 2014 Jun 15;125:116–9.
[20] Kaw AK. Mechanics of composite materials. 2nd edn. Boca Raton, FL: Taylor & Francis; 2006. p. 466. (Mechanical engineering).
[21] Quadrini F, Bellisario D, Matteo Tedde G, Santo L. Shape memory polymer composites for long-term exposure to space environment. Adv Mater Lett. 2019 Dec 1;10(12):903–6.
[22] Eskizeybek V, Avci A, Gülce A. The Mode I interlaminar fracture toughness of chemically carbon nanotube grafted glass fabric/epoxy multi-scale composite structures. Compos Part Appl Sci Manuf. 2014 Aug 1;63:94–102.
[23] Gemi L, Kara M, Avci A. Low velocity impact response of prestressed functionally graded hybrid pipes. Compos Part B Eng. 2016 Dec 1;106:154–63.
[24] Song YS, Youn JR. Influence of dispersion states of carbon nanotubes on physical properties of epoxy nanocomposites. Carbon. 2005 Jun 1;43(7):1378–85.
[25] Rathore DK, Prusty RK, Kumar DS, Ray BC. Mechanical performance of CNT-filled glass fiber/epoxy composite in in-situ elevated temperature environments emphasizing the role of CNT content. Compos Part Appl Sci Manuf. 2016 May 1;84:364–76.
[26] Wang M, Xu YG, Qiao P, Li ZM. A two-dimensional elasticity model for bending and free vibration analysis of laminated graphene-reinforced composite beams. Compos Struct. 2019 Mar 1;211:364–75.
[27] Wang E, Dong Y, Islam MZ, Yu L, Liu F, Chen S, et al. Effect of graphene oxide-carbon nanotube hybrid filler on the mechanical property and thermal response speed of shape memory epoxy composites. Compos Sci Technol. 2019 Jan 5;169:209–16.
[28] Nejati M, Asanjarani A, Dimitri R, Tornabene F. Static and free vibration analysis of functionally graded conical shells reinforced by carbon nanotubes. Int J Mech Sci. 2017 Sep 1;130:383–98.
[29] Ghasemi AR, Mohandes M, Dimitri R, Tornabene F. Agglomeration effects on the vibrations of CNTs/fiber/polymer/metal hybrid laminates cylindrical shell. Compos Part B Eng. 2019 Jun 15;167:700–16.
[30] Teng J, Wang Z, Liu J, Sun X. Effect of dynamic vulcanization system on the thermodynamics and shape memory properties of TPI/HDPE hybrid shape memory polymers. Eur Polym J. 2020 Jun 5;132:109707.
[31] Rajak D, Pagar D, Kumar R, Pruncu C. Recent progress of reinforcement materials: A comprehensive overview of composite materials. J Mater Res Technol. 2019 Oct 3;8:6354–74.
[32] Tung TK, Surdenas J. Buckling of rectangular orthotropic plates under biaxial loading. J Compos Mater. 1987 Feb 1;21(2):124–8.
[33] Lal A, Markad K. Thermo-mechanical post buckling analysis of multiwall carbon nanotube-reinforced composite laminated beam under elastic foundation. Curved Layer Struct. 2019 Jan 1;6(1):212–28.
[34] Ko WL. Anomalous buckling characteristics of laminated metal-matrix composite plates with central square holes. Edwards, Calif.: Springfield, VA: National Aeronautics and Space Administration, Dryden Flight Research Center; National Technical Information Service, distributor; 1998. p. 1. (NASA/TP).
[35] Seifi R, Khoda-yari N, Hosseini H. Study of critical buckling loads and modes of cross-ply laminated annular plates. Compos Part B Eng. 2012 Mar 1;43(2):422–30.
[36] Pai PF, Naghshineh-Pour AH, Schulz MJ, Chung J. Dynamic characteristics and buckling strength of composite-repaired aluminum plates. Finite Elem Anal Des. 1998 Jan 3;28(3):255–75.
[37] Ghaleb ZA, Mariatti M, Ariff ZM. Properties of graphene nanopowder and multi-walled carbon nanotube-filled epoxy thin-film nanocomposites for electronic applications: The effect of sonication time and filler loading. Compos Part Appl Sci Manuf. 2014 Mar 1;58:77–83.
[38] Drakonakis VM, Aureli M, Doumanidis CC, Seferis JC. Modulus–density negative correlation for CNT-reinforced polymer nanocomposites: Modeling and experiments. Compos Part B Eng. 2015 Mar 1;70:175–83.
[39] Prusty RK, Rathore DK, Shukla MJ, Ray BC. Flexural behaviour of CNT-filled glass/epoxy composites in an in-situ environment emphasizing temperature variation. Compos Part B Eng. 2015 Dec 15;83:166–74.

[40] Nagar S, Sharma K, Kukreja N, Shukla MK. Micromechanical and experimental analysis of mechanical properties of graphene/CNT epoxy composites. Mater Today Proc. 2020 Jan 1;26:1855–63.
[41] Özben T. Analysis of critical buckling load of laminated composites plate with different boundary conditions using FEM and analytical methods. Comput Mater Sci. 2009 Jun 1;45(4):1006–15.
[42] Markad KM, Das V, Lal A. Deflection and stress analysis of piezoelectric laminated composite plate under variable polynomial transverse loading. AIP Adv. 2022 Aug 25;12(8):085024.